

Original Article

Quantitative Conductivity Estimation Error due to Statistical Noise in Complex B_1^+ Map

Jaewook Shin¹, Joonsung Lee², Min-Oh Kim¹, Narae Choi¹, Jin Keun Seo³, Dong-Hyun Kim¹

¹Department of Electrical and Electronic Engineering, Yonsei University, Seoul, Korea

²SIRIC, Yonsei University, Seoul, Korea

³Department of Computer Science & Engineering, Yonsei University, Seoul, Korea

Purpose : In-vivo conductivity reconstruction using transmit field (B_1^+) information of MRI was proposed. We assessed the accuracy of conductivity reconstruction in the presence of statistical noise in complex B_1^+ map and provided a parametric model of the conductivity-to-noise ratio value.

Materials and Methods: The B_1^+ distribution was simulated for a cylindrical phantom model. By adding complex Gaussian noise to the simulated B_1^+ map, quantitative conductivity estimation error was evaluated. The quantitative evaluation process was repeated over several different parameters such as Larmor frequency, object radius and SNR of B_1^+ map. A parametric model for the conductivity-to-noise ratio was developed according to these various parameters.

Results: According to the simulation results, conductivity estimation is more sensitive to statistical noise in B_1^+ phase than to noise in B_1^+ magnitude. The conductivity estimate of the object of interest does not depend on the external object surrounding it. The conductivity-to-noise ratio is proportional to the signal-to-noise ratio of the B_1^+ map, Larmor frequency, the conductivity value itself and the number of averaged pixels. To estimate accurate conductivity value of the targeted tissue, SNR of B_1^+ map and adequate filtering size have to be taken into account for conductivity reconstruction process. In addition, the simulation result was verified at 3T conventional MRI scanner.

Conclusion: Through all these relationships, quantitative conductivity estimation error due to statistical noise in B_1^+ map is modeled. By using this model, further issues regarding filtering and reconstruction algorithms can be investigated for MREPT.

Index words : MREPT · Conductivity mapping · Noise analysis

INTRODUCTION

Magnetic resonance electric property tomography

- Received; August 19, 2014 • Revised; September 30, 2014
- Accepted; October 2, 2014

This work was supported by the National Research Foundation of Korea (NRF) grant funded by the Korea government (MEST) (No. 2012-009903).

Corresponding author : Dong-Hyun Kim, Ph.D.

Department of Electrical and Electronic Engineering, Yonsei University, 134 Sinchon-dong, Seodamun-gu, Seoul 120-749, Korea.

Tel. 82-2-2123-5874, Fax. 82-2-313-2879

E-mail : donghyunkim@yonsei.ac.kr

This is an Open Access article distributed under the terms of the Creative Commons Attribution Non-Commercial License (<http://creativecommons.org/licenses/by-nc/3.0/>) which permits unrestricted non-commercial use, distribution, and reproduction in any medium, provided the original work is properly cited.

(MREPT) was recently re-introduced to noninvasively image the distribution of electric property in human body at Larmor frequency (1, 2). Electric conductivity has been proposed to be used in diagnostic applications (3–6) and for specific absorption rate (SAR) calculation (7). Over homogeneous regions, the relationship between the electric properties and magnetic fields can be simplified as a Helmholtz equation of the radiofrequency (RF) transmit field, B_1^+ . In MREPT, the electrical properties distribution can be reconstructed from B_1^+ field information by using the Helmholtz equation. The B_1^+ magnitude and phase information is acquired separately using different sequences. For example, B_1^+ magnitude mapping techniques such as actual flip angle imaging (AFI) (8),

multiple TR B1/T1 mapping (MTM) (9), double angle method (DAM) (10) and Bloch-Siegert method (11) have been proposed and B_1^+ phase map has been generally measured using half the phase acquired by a spin echo (2) or multi-echo gradient echo sequence (12) under the assumption that the B_1^+ transmit and receive phases are identical. In addition, conductivity reconstruction using only the B_1^+ phase has been introduced (13) and widely used (14, 15), however it can provide accurate conductivity values under the assumption that the spatial variation of B_1^+ magnitude is negligible. For all these applications and measurements, the conductivity value is needed to be estimated under an acceptable error level.

In MREPT reconstruction process, systemic and statistic error exists. First, systemic error occurs due to invalidity of the spatial homogeneity assumption and of the assumption of equality between B_1^+ phase (θ_1^+) and B_1^- phase (θ_1^-). When using the Helmholtz equation, boundary artifact is presented at tissue boundaries because of the invalidity of the spatial homogeneity assumption. In a previous study (16), rigorous mathematical error analysis about the boundary artifact was performed and numerical equation which takes into account the inhomogeneity was derived from time-harmonic Maxwell equation. Also, the half value of measured phase, $\frac{1}{2}\theta_1^m = \frac{1}{2}(\theta_1^+ + \theta_1^-) \approx \theta_1^+$, is assumed as the B_1^+ phase due to the assumption regarding the equality of phase. However, as the main field (B_0) increases, assumption about the phase equality becomes weaker and reconstructed conductivity map becomes inhomogeneous even over homogeneous regions (17). In the case of B_1^+ phase based conductivity reconstruction, an additional systemic error occurs inside the object due to the non-negligible B_1^+ magnitude variation.

The second error occurs due to the statistical noise in the B_1^+ map acquired. This statistic error is a fundamental limiting factor for application of quantitative conductivity mapping because the Laplacian operator, a secondary spatial derivative on the Euclidean space, used in the Helmholtz equation amplifies the statistical noise in the B_1^+ map. To overcome these limitations, filtering, fitting and integral techniques are applied for conductivity imaging process (2, 13, 14). However, analysis about quantitative error due to noise in B_1^+ map has not

been performed prior to the application of these mentioned techniques. Therefore, in this study, quantitative conductivity estimation error due to the presence of statistical noise in the B_1^+ map is analyzed and the factors that affect the variation of conductivity estimation inside tissue are examined. In addition, a numerical monomial form is suggested as approximate model for quantitative conductivity estimation error. The results of this study can be utilized for optimal filter design, comparison among reconstruction methods and examination of validity in clinical applications.

MATERIALS AND METHODS

Simulation model and Conductivity estimation method

Noiseless B_1^+ field distribution of radio frequency (RF) transmit field at Larmor frequency was calculated using the Bessel boundary matching (BBM) method (18) which is a very fast electromagnetic (EM) simulation method for simple segmented models. The BBM method was implemented in MATLAB (The Mathworks, Inc., Natick, MA, USA). The numerical simulation phantom shown in Fig. 1 was an infinitely long cylinder placed at the iso-center of a 32 rod quadrature coil and the locations of the RF shield and

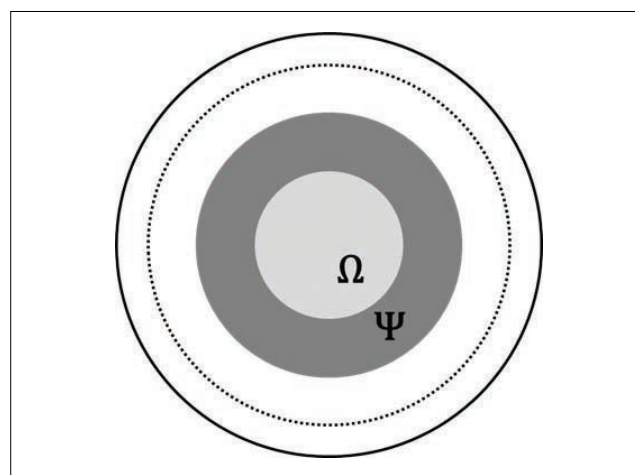


Fig. 1. Cross-section of infinitely long cylinder simulation model. MRI scanner was implemented RF shield (black line) and 32 rod quadrature coil (black dashed line). Simulation phantom (light gray region Ω) and surrounding tissue (dark gray region Ψ) was located at iso-center of MRI scanner.

RF coil were fixed at radius of 45 cm and 16.5 cm, respectively. The simulated phantom's radius, conductivity, permittivity and Larmor frequency was fixed to 5.5 cm, 1.0 S/m, $80\epsilon_0$, and 128 MHz, respectively, unless otherwise mentioned. The phantom was assumed to be surrounded by a different material having radius of 11 cm. The resolution of the generated B_1^+ map was 1 mm by 1 mm.

Conductivity $\sigma(r)$ was evaluated using the Helmholtz equation of Eq. 1 which can be induced from Maxwell's equation. The Laplacian operator was calculated using the surrounding four pixels in the discrete image domain. In addition, conductivity reconstruction using only the phase information was performed using Eq. 2 which is the 2D formation of B_1^+ phase based method at a single point (13).

$$\sigma(r) = \text{Re} \left\{ \frac{\nabla^2 B_1^+(r)}{i\omega\mu_0 B_1^+(r)} \right\} \quad [1]$$

$$\sigma(r) \approx \frac{\nabla^2 \theta_1^+(r)}{\mu_0 \omega} \quad [2]$$

Afterwards, as in Eq. 3, conductivity estimation of a segmented region, \mathcal{Q} , was calculated by averaging the evaluated conductivity values excluding the boundaries, since the applicability of Eq. 1 and 2 are guaranteed only over homogeneous regions where area of the region is $S_{\mathcal{Q}}$.

$$\hat{\sigma} = \frac{\int_{\mathcal{Q}} \sigma(r) dS}{S_{\mathcal{Q}}} \quad [3]$$

Quantitative Conductivity Estimation Error Analysis

To investigate the relationship between quantitative conductivity estimation error and statistical noise in the B_1^+ map, Gaussian noise was added to the B_1^+ map prior to MREPT processing. In reality, it is necessary to separately consider the noise in the B_1^+ magnitude and phase maps due to the separate acquisition of these maps. Statistical noise in B_1^+ phase map shows Gaussian distribution for $\text{SNR} \gg 1$ (19) but, statistical noise in B_1^+ magnitude map shows diverse distribution depending on the B_1^+ mapping method (20). However, in this simulation study, the noise in B_1^+ magnitude map was assumed to be Gaussian distributed which seems reasonable since we focus on quantitative

conductivity estimation error not to pattern of the error. Quantitative conductivity estimation error was defined in terms of the normalized root mean square error (NRMSE) obtainable from Eq. 4 with the real conductivity value σ_{real} evaluated using N trials of Monte Carlo simulations. However, in the case of B_1^+ phase based conductivity reconstruction, reconstructed conductivity value inside homogeneous regions includes systemic error. So, to consider only the effect of statistical noise, the systemic error was disregarded in this case.

$$\text{NRMSE} = \frac{\sqrt{\sum_{i=1}^N (\sigma_{\text{real}} - \hat{\sigma}_i)^2 / N}}{\sigma_{\text{real}}} \quad [4]$$

A conductivity-to-noise ratio (σNR) is defined which is the real conductivity value divided by the standard deviation γ_{noise} of the statistical noise in the conductivity map (Eq. 5). In the case of a 1 mm radius object which is identical to the simulated image spatial resolution, since the homogeneous region excluding the boundary is just one pixel, the standard deviation γ_{noise} is equal to the root mean square error (RMSE). Then the σNR is equal to $1/\text{NRMSE}_{1\text{ mm}}$, where $\text{NRMSE}_{\text{Rmm}}$ represents NRMSE value over a target tissue of R millimeter radius. Although, the σNR can vary according to size and location of the target object, a previous study (13) showed the spatial dependency of conductivity evaluation error to be marginal. Here we can regard $1/\text{NRMSE}_{1\text{ mm}}$ as the general σNR over an object since the resolution of the simulated B_1^+ map is 1 mm. Thus we refer to $\text{NRMSE}_{1\text{ mm}}$ as the standard NRMSE.

$$\begin{aligned} \sigma\text{NR} &\equiv \frac{\sigma_{\text{real}}}{\gamma_{\text{noise}}} = \frac{\sigma_{\text{real}}}{\sqrt{\sum_{\mathcal{Q}} (\sigma_{\text{real}} - \sigma(r))^2} / N_{\mathcal{Q}}} \\ &\cong \frac{\sigma_{\text{real}}}{\sqrt{\sum_{i=1}^N (\sigma_{\text{real}} - \hat{\sigma}_i)^2} / N} = \frac{1}{\text{NRMSE}_{1\text{ mm}}} \end{aligned} \quad [5]$$

(Simulation Variable A) Magnitude and phase noise

As referred in the introduction, SNR of B_1^+ map is one of dominant factors for the accurate estimation of conductivity. In MR scanner, the B_1^+ magnitude and

phase are measured separately using different sequences, and thus the accuracy of B_1^+ magnitude and the accuracy of B_1^+ phase are different. In this work, the effect of complex noise in B_1^+ map on conductivity estimation was investigated. Additionally, to investigate the dependency of conductivity estimation due to noise in separately acquired B_1^+ magnitude and phase maps, the estimation error due to B_1^+ magnitude noise or phase noise was calculated individually. To evaluate the accuracy of conductivity estimates with noisy B_1^+ maps, we performed EM simulations to obtain noiseless B_1^+ maps. Then, we considered four different cases of noisy B_1^+ maps generated by adding Gaussian noises.

1. Noisy B_1^+ complex – adding complex Gaussian noise to B_1^+ complex.
2. Noisy B_1^+ magnitude and noiseless B_1^+ phase – adding real Gaussian noise to B_1^+ magnitude.
3. Noiseless B_1^+ magnitude and noisy B_1^+ phase – argument of noisy B_1^+ complex.
4. Noisy B_1^+ magnitude and noisy B_1^+ phase (fixed noise level) – combining noisy B_1^+ magnitude (case 2) and noisy B_1^+ phase (case 3) using Euler's formula

Specifically, for B_1^+ complex and B_1^+ magnitude, the NRMSE of conductivity estimates was evaluated by varying the SNR of B_1^+ . The SNR of B_1^+ complex and magnitude map can be defined as the average intensity of B_1^+ inside the region of interest over the standard deviation of noise. However, for B_1^+ phase, the above definition of SNR was not used directly since the phase itself is not absolute, but phase synchronization at an interval of 2π . The standard deviation of phase

noise is a reciprocal of SNR in MR images (19). Thus, for B_1^+ phase, the NRMSE of conductivity estimates was evaluated by varying the SNR of MR images.

In addition, to investigate the specific effect of statistical noise in B_1^+ magnitude on conductivity estimation, the NRMSE of conductivity estimates was evaluated by varying the SNR of B_1^+ magnitude according to conductivity value and B_1^+ phase with fixed noise level.

(Simulation Variable B) Tissue characteristic & Larmor frequency

The effect of tissue related variables on conductivity estimation was examined. There are many variables associated with tissue, but, in this simulation, only three variables which cause change to the transmit field distribution were dealt with. In addition, the NRMSE value was calculated from conductivity estimates simulated from B_1^+ maps using human tissue conductivity values previously reported from an ex-vivo study (21). These were done for different frequency values. The specific methods are mentioned below.

1. Surrounding tissue conductivity

The NRMSE from the tissue of interest (\mathcal{Q}), which was surrounded by another tissue (Ψ) at a radius of 11 cm (Fig. 1), was calculated. To examine the effect of the surrounding tissue on the reconstructed conductivity, the SNR level of the B_1^+ map inside the tissue of interest was fixed to 100 and the conductivity of the surrounding tissue (σ_{out}) was increased.

Table 1. Literature Electric Conductivity Value for Seven Types of Human Tissue. Literature Values were Used to Generate the Complex Transmit Field Using BBM Method

| | Conductivity (S/m) | | | Relative permittivity | | |
|--------------|--------------------|----------|---------|-----------------------|--------|--------|
| | 1.5T | 1.5T | 3T | 1.5T | 3T | 7T |
| CSF | 2.066 | 2.066 | 2.143 | 97.312 | 84.041 | 72.734 |
| Prostate | 0.88486 | 0.88486 | 0.92639 | 84.527 | 72.128 | 64.837 |
| Heart | 0.67841 | 0.67841 | 0.76609 | 106.51 | 84.257 | 69.307 |
| Gray Matter | 0.51086 | 0.51086 | 0.58672 | 97.429 | 73.52 | 60.022 |
| Liver | 0.44797 | 0.44797 | 0.51089 | 80.56 | 64.251 | 53.512 |
| White Matter | 0.2915 | 0.2915 | 0.34214 | 67.836 | 52.534 | 43.776 |
| Fat | 0.035275 | 0.035275 | 0.03687 | 6.5064 | 5.9215 | 5.634 |

2. Larmor frequency

Electric property of human tissues depends on frequency. Therefore, it will vary with the Larmor frequency of main magnetic field, f . Using electric property values from previous study (21) (Table 1), the NRMSE was calculated for seven different tissue types at three Larmor frequencies, 64 MHz, 128 MHz and 300 MHz. Fat, white matter (WM), gray matter (GM), prostate, cerebrospinal fluid (CSF), heart and liver were selected for the simulations. Here, these human tissues were modeled as cylindrical shapes with fixed radius of 5 mm (Fig. 1).

3. Tissue size

This simulation was performed using different sizes of simulation phantom whose radius was altered from 1 mm to 10 mm. Over a homogeneous conductivity region, the conductivity map obtained from the aforementioned MREPT process was averaged to estimate the conductivity value. The number of pixels being averaged (N_A) used in the conductivity estimation, is approximately proportional to the area of the phantom. Therefore, N_A equal 1, 5, 13, 49, 253 for phantom of radius 1 mm, 2 mm, 3 mm, 5 mm, 10 mm, respectively.

Parametric Modeling of the error in the conductivity estimate

The relationships between the error in the conduc-

tivity estimates and other imaging parameters were investigated. The imaging parameters considered here are N_A , SNR of B_1^+ , f , σ_{real} , σ_{out} . For each imaging parameter, x , we modeled that the estimation error, NRMSE, is inversely proportional to a power p of x (Eq. 6).

$$\frac{1}{\text{NRMSE}} \propto x^p \quad [6]$$

To determine the power of the variable, p , the logarithm of the estimation error was fitted to a linear line of x and p was determined from the slope of the fitted line. To confirm the fitting accuracy, the R^2 (determinant coefficient) value was calculated.

Experimental study

To verify the simulation results, a cylindrical phantom (radius = 5.5 cm and height = 18 cm) was built and imaged. The phantom was filled with a mixture of 0.5% NaCl and 0.5% agar gel. The phantom conductivity measured with a conductivity meter (HI8733N, Hanna Instruments) was 0.82 S/m at 26° C. The measured conductivity value can be used to the conductivity value at 3T MRI because, in the case of saline water, the electric conductivity value is independent of frequency (22). To measure the B_1^+ magnitude, double angle method (DAM) acquired with 60°–180° and 120°–180° flip angle acquisitions was used (10). For B_1^+ phase measurement, the half value

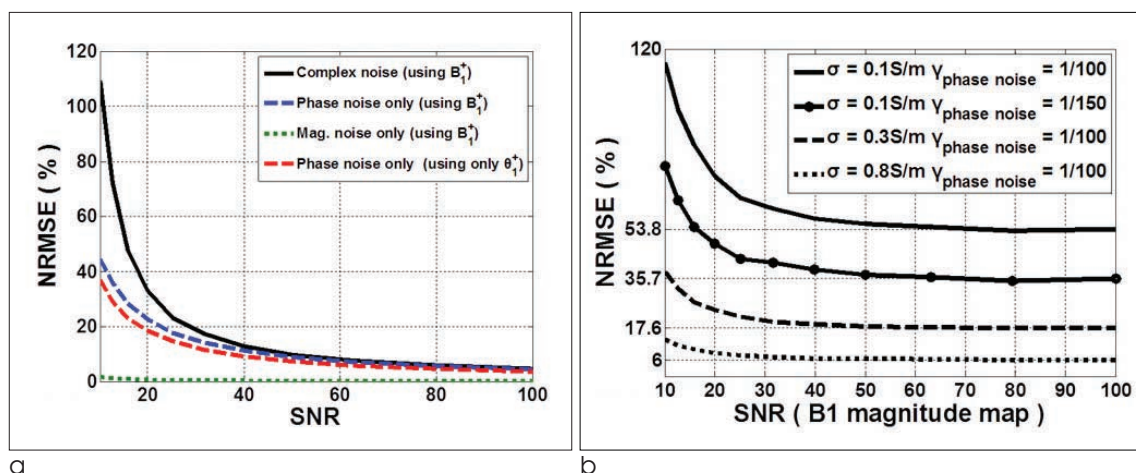


Fig. 2. Quantitative conductivity estimation error (NRMSE) graph.

a. SNR variation due to three types statistical noise using complex B_1^+ information (Eq. 1) and phase noise using only B_1^+ phase information (Eq. 2).

b. SNR variation due to B_1^+ magnitude noise with fixed level of phase noise and conductivity variation 0.1 to 0.8.

of the phase of a turbo spin echo (TSE) sequence was used. The imaging parameters were as follows: $TR_{TSE}/TE_{TSE} = 800/20$ ms, $TR_{DAM}/TE_{DAM} = 2500/20$ ms, $FOV = 128 \times 128$ mm², resolution = 1.0×1.0 mm², slice thickness = 4 mm, 9 slices, and single channel quadrature transmit/receive coil was used. The SNR of B_1^+ magnitude map was calculated using the law of error propagation similar to the approach in (9) and gave a value of 48. In the case of TSE for B_1^+ phase measurement; acquisitions were repeated to gather 40 data sets, each 10 data sets were separately averaged to make the SNR vary from 80 to 220. All experiments were performed on a 3T Trio TIM system (Siemens Medical Solutions, Erlangen, Germany). The results were compared using the same size phantom with same SNR variation as the simulations.

RESULTS

The comparison of conductivity estimation due to three types of noise-magnitude, phase and complex noise type-is illustrated in Fig. 2 to evaluate which error component is most influential. It seems that the magnitude noise in B_1^+ rarely affects to the conductivity estimation (less than 5% error) according to the green-dot line in Fig. 2a. However, conductivity estimation is sensitive to complex and phase noise as shown in the blue-dash and black-solid line. Hence, it can be interpreted that the phase information is dominant for general conductivity reconstruction method which is in agreement with previous study (13).

When SNR varies from 10 to 40, the effect of complex noise which contains magnitude and phase noise is more influential than the effect of only phase noise (Fig. 2a). Thus, it can be interpreted that sensitivity of conductivity estimation to magnitude noise increases as SNR decreases in the B_1^+ magnitude. In detail, Fig. 2b shows the NRMSE curves with fixed phase noise level converge to each minimum NRMSE values as conductivity changes. This convergence means that it is not necessary to increase magnitude SNR more than a specific conductivity-dependent level. In this study, we defined the minimum required B_1^+ magnitude level that makes the NRMSE to be within 3% difference with minimum NRMSE. This

resulted in a value of 61.6, 39.8, 24.5 for conductivity values of 0.1, 0.3, 0.8 S/m. These values were further investigated for conductivity commonly found in *in vivo* at 3T and were summarized in Table 2. Note that these values are independent of phase noise level (Fig. 2b). Using the p -th degree parametric model, the proportionality relationship between $1/NRMSE$ and SNR of complex B_1^+ map ($SNR_{B_1^+}$) was fitted to first degree ($p=1$) as in Eq. 7 with 0.9559 R^2 value.

$$\frac{1}{NRMSE} \propto SNR_{B_1^+} \quad [7]$$

As shown in Fig. 2a, the graphs of conductivity estimation errors due to B_1^+ phase and complex noise show comparable NRMSE value when each SNR is higher than about 40. Therefore, SNR of the B_1^+ map in Eq. 7 can be regarded as the SNR of the acquired image for B_1^+ phase mapping.

The red dashed line in Fig. 2a shows conductivity estimation error when using phase based method. The error graph shows conductivity reconstruction using phase based method is less sensitive to statistical noise in B_1^+ phase map than using both B_1^+ magnitude and phase information. However, conductivity reconstruction using phase based method contains additional systemic error since it neglects variation of B_1^+ magnitude. When phase based method was used for cylindrical object with the radius of 5.5 cm, conductivity value was 20% overestimated as an additional systemic error.

Fig. 3 shows the error in the conductivity estimates for seven types of tissues with the fixed radius of 5 mm for different Larmor frequencies. In general, the accuracy of conductivity estimation increases along

Table 2. Minimum Required SNR of B_1^+ Magnitude Map to Minimize Quantitative Conductivity Estimation Error (NRMSE) According to the Electric Conductivity Value of Target Tissue

| Conductivity (S/m) | Minimum SNR of B_1^+ magnitude for within 3% difference with minimum NRMSE |
|--------------------|--|
| 0.15 | 53.7 |
| 0.25 | 43.7 |
| 0.35 | 36.3 |
| 0.5 | 30.9 |
| 1.0 | 21.9 |

Larmor frequency under fixed SNR. This phenomenon can be explained by the fluctuation of B_1^+ magnitude and phase distribution (23, 24) which increases with Larmor frequency and makes the estimated conductivity value immune against amplified noise in the Laplacian operator. Also, the accuracy of conductivity estimates increases as tissue conductivity increases. Therefore, these two factors, Larmor frequency and conductivity value, can be represented to be directly proportional to $1/\text{NRMSE}$ value (Eq. 8).

$$\frac{1}{\text{NRMSE}} \propto f \sigma_{\text{tissue}} \quad [8]$$

The fitting of the above results gave a R^2 value of 0.996 and 0.9999 for B_0 and σ of tissue respectively. In calculating the fitting degree for Larmor frequency, the dependence of tissue conductivity on frequency was taken into account. As an example, if the conductivity is estimated using Eq. 1 at 128 MHz, the

minimum radius of the homogeneous region required for NRMSE to be less than 10% given a single slice of B_1^+ map with a spatial resolution of 1 mm and the SNR of 100, are about 128 mm (WM), 99 mm (Liver), 90 mm (GM), 73.8 (Heart), 64.5 mm (Prostate), 33.4 mm (CSF).

To assess the influence of the presence of conductivity material at the outer tissue, the results of evaluated NRMSE with various conductivity values at the outer tissue is seen in Fig. 4a. As seen, the conductivity of the outer tissue has no effect on conductivity estimation of the inner tissue for fixed SNR at the region of interest. As a result, the power of simulation variable σ_{out} can be estimated to 0 thus the term which related to σ_{out} can be removed.

Fig. 4b shows the relationship between the conductivity estimation error and radius of the tissue. As the radius of the estimation region increases, N_A increases. As a result, the conductivity estimation error gradually

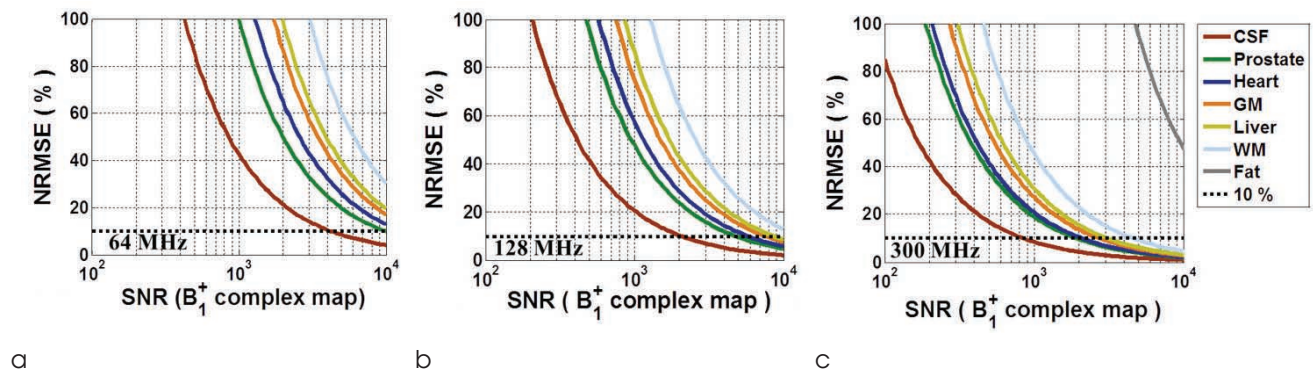


Fig. 3. Error in the conductivity estimation for seven types of tissues at the radius of 5 mm and B_0 intensity 1.5T (a), 3T (b) and 7T (c). Fat (dark gray line) is observed only 7T B_0 intensity within the given SNR range, $10^2 \sim 10^4$.

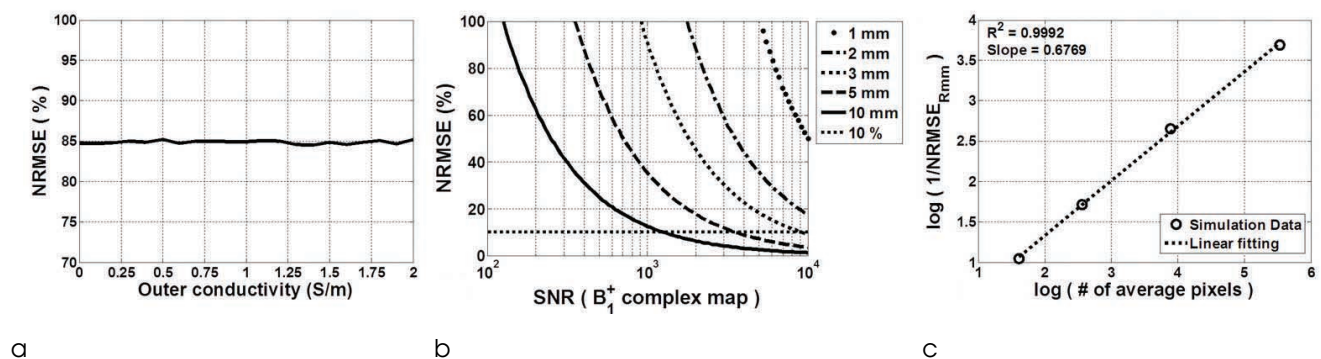


Fig. 4. Quantitative conductivity estimation error due to (a) electric conductivity of outer surrounding tissue and (b) radius of homogeneous region. (c) NRMSE fitting result according to the number of averaged pixels that is almost proportional to square radius with 0.9992 R^2 (determinant coefficient) value.

decreases. More specifically, the NRMSE ratio between 1 mm radius and the others can be found to be $\frac{NRMSE_{2\text{ mm}}}{NRMSE_{1\text{ mm}}} : \frac{NRMSE_{3\text{ mm}}}{NRMSE_{1\text{ mm}}} : \frac{NRMSE_{5\text{ mm}}}{NRMSE_{1\text{ mm}}} : \frac{NRMSE_{10\text{ mm}}}{NRMSE_{1\text{ mm}}} \approx 14.14 : 7.25 : 2.83 : 1$. This ratio is inversely proportional to the N_A to a degree of 2/3 (0.9992 of R^2 value, Fig. 4c). Since N_A is almost proportional to square of the radius, the NRMSE for a R_{mm} object is related to the standard NRMSE_{1 mm} as the following: .

$$NRMSE_{R_{\text{mm}}} = \frac{NRMSE_{1\text{ mm}}}{N_A^{2/3}} \propto \frac{NRMSE_{1\text{ mm}}}{R^{4/3}} \quad [9]$$

The conductivity estimation process is analogous to a kind of filtering process since the homogeneous region with radius R_{mm} is averaged to estimate σ and NRMSE. Thus, $1/NRMSE_{R_{\text{mm}}}$ of estimated conductivity value can be the σNR after filtering.

In summary, quantitative conductivity estimation error due to statistical noise can be represented as in Eq. 10. In addition, the conductivity-to-noise-ratio averaged over an R_{mm} radius ($\sigma NR_{R_{\text{mm}}}$) can be defined as in Eq. 11.

$$\sigma NR = \frac{1}{NRMSE_{1\text{ mm}}} = \frac{SNR_{B_1^+} f \sigma_{\text{tissue}}}{K} \quad [10]$$

$$\sigma NR_{R_{\text{mm}}} \equiv \frac{1}{NRMSE_{R_{\text{mm}}}} = \frac{SNR_{B_1^+} f \sigma_{\text{tissue}} N_A^{2/3}}{K} \quad [11]$$

The unit for frequency (f) is in MHz and σ_{tissue} is in S/m. Here, the proportional constant K is added, which directly relates to the σNR and the parameters considered. In our simulation model, the value of K was approximately 640,000. However, this value will

depend on many factors such as object shape and location, coil size, etc. The $SNR_{B_1^+}$ can be influenced by the B_0 value. Here, we assumed that the parameters $SNR_{B_1^+}$ and B_0 value are independent.

In MREPT, given a fixed Larmor frequency and the conductivity value of target tissue (σ_{tissue}), the dependent parameters are $SNR_{B_1^+}$ and the number of being averaged pixels (N_A). Therefore, the principle of Eq. 11 can be utilized for conductivity mapping. As an example, if we consider a malignant liver tissue of 1 mm object whose conductivity value is 0.66 S/m (at 100 MHz, (3)) and a conductivity map with $\sigma NR = 2$ is required, the $SNR_{B_1^+}$ needed has to be approximately 19,000. In reality, to overcome the lack of SNR, a 22 mm radius homogeneous region is required to estimate the conductivity value with $\sigma NR_{R_{\text{mm}}} = 2$ using a 100 $SNR_{B_1^+}$. Therefore, when the conductivity of target tissue, maximum available $SNR_{B_1^+}$ and B_0 field of the MRI scanner is fixed, the minimum size of detectable tissue using the MREPT process with an averaging filter is determined.

Finally, the principles obtained from the simulation results were compared to experiment study (Fig. 5). According to Table 2, the SNR of the acquired B_1^+ magnitude map of 48 was sufficient to minimize NRMSE value for a phantom with conductivity value of 0.82 S/m. Thus, the NRMSE value was calculated according to the SNR of the image used for acquiring B_1^+ phase map (Fig. 5a). The error graphs obtained from simulation and experiment show similar results. Note that the experiment results contain systemic error due to invalidity of the assumption of equality

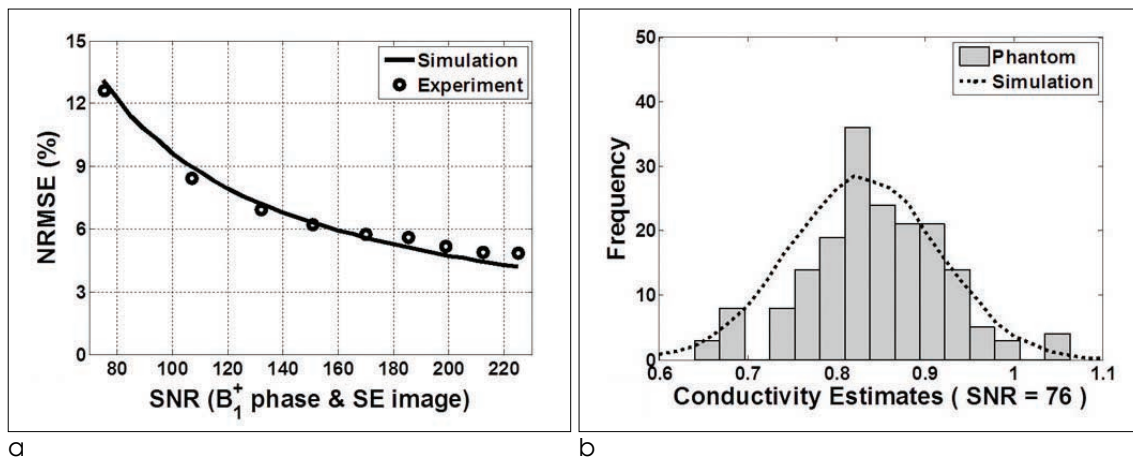


Fig. 5. a. Comparison of the error between simulation result (black bold line) and phantom experimental result (black dash line). **b.** Histogram of estimated conductivity value in experiment result (SNR of SE image = 80).

between θ_1^+ and θ_1^- . However, the effect of this systemic error was insignificant for conductivity estimation because of the spatially symmetric pattern of this error which vanishes by averaging process (17). Figure 5b shows the histogram of estimated conductivity values which shows similarity between the distribution of conductivity estimation value for simulation and experiment result.

DISCUSSION

Reconstruction of conductivity image using MREPT process suffers from systemic and statistic error. Especially, statistical noise in B_1^+ map restricts the feasibility of MREPT. Hence, in this study, the relationship between quantitative conductivity estimation error and the parameters that affect the MREPT process was investigated and modeled as in Eq. 11. The systemic constant K can be different value according to the shape of tissue and transmit, receive coil, but the general tendency shown in this study holds.

For quantitative conductivity imaging, $SNR_{B_1^+}$ is the most dominant factor because the Larmor frequency and conductivity of target tissue are almost uncontrollable factors. Thus, in the step of B_1^+ map acquisition, sufficient $SNR_{B_1^+}$ have to be guaranteed. Also, SNR of B_1^+ magnitude and phase map have to be considered separately because the phase and magnitude of the RF transmit field, B_1^+ , is generally acquired using different sequences. In the case of B_1^+ magnitude map, the minimum required SNR of B_1^+ magnitude for maximizing the SNR of conductivity map depends on the conductivity value according to Table 2. The minimum required SNR may change according to B_1^+ magnitude mapping method due to the different distribution of noise in B_1^+ magnitude map method however it will not vary significantly from the values in Table 2. Therefore, the acquisition time of B_1^+ magnitude map should be fixed to a minimum to achieve the SNR required and the additional scan time can be used for achieving higher SNR of the acquired image for B_1^+ phase mapping.

To overcome the sensitivity to statistical noise in B_1^+ map, a filter was applied to the conductivity reconstruction process (2). In this study, the conductivity estimation process using the average of the

reconstructed conductivity value inside a homogeneous region roughly shows the effect of filtering. From statistics, there is an \sqrt{N} SNR improvement when N number of pixels with independent random noise from a homogeneous region is averaged. However, in MREPT, there is an additional SNR improvement ($N^{2/3}$ in Eq. [9]) because the Laplacian operator can be regarded as an average over several pixels, i.e., the center and the surrounding pixels. Note that the minimum size of a detectable target tissue is regulated according to the filter size.

Higher Larmor frequency value also reduces conductivity reconstruction error because, as mentioned, the increase of Larmor frequency yields rapid spatial variation of B_1^+ phase inside the object (24). However, in case of high B_0 such as 7T, the assumption about the equality of θ_1^+ and θ_1^- is broken and this results in the increment of systemic error. Hence, in using B_1^+ map acquired at high field MRI scanners, the detection and correction of systemic errors in conductivity map is required.

Through all these relationships, quantitative conductivity estimation error due to statistical noise in B_1^+ map can be modeled as in Eq. 11. The equation can be used to find necessary $SNR_{B_1^+}$ and filter size according to the required conductivity differences between, for example, normal and malignant tissue with a certain size. In addition, using this method, further issues regarding filtering and reconstruction algorithms can be investigated for MREPT.

Acknowledgements

This work was supported by the National Research Foundation of Korea (NRF) grant funded by the Korea government (MEST) (No. 2012-009903).

References

1. Haacke EM, Petropoulos LS, Nilges EW, Wu DH. Extraction of conductivity and permittivity using magnetic resonance imaging. *Phys Med Biol* 1991;36:723-734
2. Katscher U, Voigt T, Findekklee C, Vernickel P, Nehrke K, Dossel O. Determination of electric conductivity and local SAR via B_1 mapping. *IEEE Trans Med Imaging* 2009;28:1365-1374
3. Joines WT, Zhang Y, Li C, Jirtle RL. The measured electrical properties of normal and malignant human tissues from 50 to 900 MHz. *Med Phys* 1994;21:547-550
4. Schaefer M, Gross W, Ackemann J, Gebhard MM. The complex dielectric spectrum of heart tissue during ischemia. *Bioelectro-*

- chemistry 2002;58:171-180
5. Haemmerich D, Staelin ST, Tsai JZ, Tungjitkusolmun S, Mahvi DM, Webster JG. In vivo electrical conductivity of hepatic tumours. *Physiol Meas* 2003;24:251-260
6. Fallert MA, Mirotznik MS, Downing SW, et al. Myocardial electrical-impedance mapping of ischemic sheep hearts and healing aneurysm. *Circulation* 1993;87:199-207
7. Voigt T, Homann H, Katscher U, Doessel O. Patient-individual local SAR determination: in vivo measurements and numerical validation. *Magn Reson Med* 2012;68:1117-1126
8. Yarnykh VL. Actual flip-angle imaging in the pulsed steady state: a method for rapid three-dimensional mapping of the transmitted radiofrequency field. *Magn Reson Med* 2007;57:192-200
9. Voigt T, Nehrke K, Doessel O, Katscher U. T1 corrected B1 mapping using multi-TR gradient echo sequences. *Magn Reson Med* 2010;64:725-733
10. Stollberger R, Wach P. Imaging of the active B1 field in vivo. *Magn Reson Med* 1996;35:246-251
11. Sacolick LI, Wiesinger F, Hancu I, Vogel MW. B1 mapping by Bloch-Siegert shift. *Magn Reson Med* 2010;63:1315-1322
12. Kim DH, Gho SM, Choi N, Liu C. Simultaneous Electromagnetic Property Imaging using multiecho gradient echo. In: *Proceedings of the 20th Annual Meeting of ISMRM, Melbourne, Australia, 2012* p 3464
13. Voigt T, Katscher U, Doessel O. Quantitative conductivity and permittivity imaging of the human brain using electric properties tomography. *Magn Reson Med* 2011;66:456-466
14. Bulumulla SB, Lee S, Yeo DTB. Conductivity and permittivity imaging at 3.0 T. *Concept Magn Reson B* 2012;41B(1):13-21
15. van Lier AL, Brunner DO, Pruessmann KP, et al. B1(+) phase mapping at 7 T and its application for in vivo electrical conductivity mapping. *Magn Reson Med* 2012;67:552-561
16. Seo JK, Kim MO, Lee J, et al. Error analysis of nonconstant admittivity for MR-based electric property imaging. *IEEE Trans Med Imaging* 2012;31:430-437
17. van Lier AL, Voigt T, Katscher U, van den Berg CA. Comparing Electric Properties Tomography at 1.5, 3 and 7 T. In: *Proceedings of the 19th Annual Meeting of ISMRM, Montreal, Canada, 2011* p 125
18. van den Bergen B, Stolk CC, Berg JB, Lagendijk JJ, Van den Berg CA. Ultra fast electromagnetic field computations for RF multi-transmit techniques in high field MRI. *Phys Med Biol* 2009;54:1253-1264
19. Gudbjartsson H, Patz S. The Rician distribution of noisy MRI data. *Magn Reson Med* 1995;34:910-914
20. Morrell GR, Schabel MC. An analysis of the accuracy of magnetic resonance flip angle measurement methods. *Phys Med Biol* 2010;55:6157-6174
21. <http://niremf.ifac.cnr.it/tissprop/>
22. Stogryn A. Equations for calculating the dielectric constant of saline water. *IEEE Trans Microwave Theory Tech* 1971;19:733-736
23. Gabriel S, Lau RW, Gabriel C. The dielectric properties of biological tissues: II. Measurements in the frequency range 10 Hz to 20 GHz. *Phys Med Biol* 1996;41:2251-2269
24. Zypman FR. MRI electromagnetic field penetration in cylindrical objects. *Comput Biol Med* 1996;26:161-175

정량적 도전율측정의 오차와 B_1^+ map의 노이즈에 관한 분석

¹연세대학교 전기전자공학
²연세대학교 뇌심혈관질환융합연구사업단
³연세대학교 계산과학공학

신재욱¹ · 이준성² · 김민오¹ · 최나래¹ · 서진근³ · 김동현¹

목적: 자기공명 영상장치(MRI)의 송신 자기장 정보를 이용한 인체 내 도전율을 측정하는 기술이 최근 제안되었다. 송신 자기장 정보의 노이즈에 따른 도전율의 오차를 측정하고 도전율과 노이즈의 관계를 모델화 하였다.

대상과 방법: 송신 자기장의 분포는 원형 모델에 대해서 시뮬레이션을 수행하였다. 시뮬레이션으로 생성된 송신 자기장의 분포에 가우시안 노이즈를 더해준 후 정량적인 도전율 측정에 어떤 영향을 주는지 공명 주파수, 물체의 크기, 송신 자기장의 신호 대 잡음 비에 대해서 수행하였다. 각 각의 변수에 따른 도전율 대 잡음 비를 측정하여 모델화 하였다.

결과: 시뮬레이션 결과 도전율 측정은 송신 주파수의 크기 오차보다 위상 오차에 더 큰 영향을 받는 것을 보였다. 또한, 송신 자기장의 신호 대 잡음 비, 공명 주파수, 도전율 값, 평균필터의 크기에 따라서 도전율 대 잡음비가 비례하는 경향성을 보였다. 하지만, 물체를 둘러싼 외부 물질의 크기는 도전율 측정에 큰 영향을 주지 않았다. 위의 시뮬레이션 결과는 3T 임상용 MRI에서 원형 모델 팬텀에 대해서 검증되었다.

결론: 시뮬레이션을 통해 얻어진 변수와 도전율 측정의 오차와의 관계를 통해서 정량적인 도전율 측정에서 발생하는 오차를 모델화 할 수 있었다. 또한 제시된 분석 방법을 통하여 자기공명 영상 장치를 이용한 도전율 측정의 필터링 및 재구성 알고리즘의 효과를 검증 할 수 있을 것으로 보인다.

통신저자 : 김동현, (120-749) 서울시 서대문구 신촌동 134, 연세대학교 전기전자공학
 Tel. (02) 2123-5874 Fax. (02) 313-2879 E-mail: donghyunkim@yonsei.ac.kr